Proceedings of ASME Turbo Expo 2011
GT2011
June 6-10, 2011, Vancouver, British Columbia, Canada

GT2011-46328

AN INVESTIGATION OF REYNOLDS LAPSE RATE FOR HIGHLY LOADED LOW PRESSURE TURBINE AIRFOILS WITH FORWARD AND AFT LOADING

M. Eric Lyall
Air Force Institute of Technology
Wright-Patterson AFB, OH, USA

Paul I. King
Air Force Institute of Technology
Wright-Patterson AFB, OH, USA

Rolf Sondergaard
Air Force Research Laboratory
Wright-Patterson AFB, OH, USA

John P. Clark
Air Force Research Laboratory
Wright-Patterson AFB, OH, USA

Mark W. McQuilling
Saint Louis University
St. Louis, MO, USA

ABSTRACT

This paper presents an experimental and computational study of the midspan low Reynolds number loss behavior for two highly loaded low pressure turbine airfoils, designated L2F and L2A, which are forward and aft loaded, respectively. Both airfoils were designed with incompressible Zweifel loading coefficients of 1.59. Computational predictions are provided using two codes, Fluent (with k-k_l-ω model) and AFRL‟s Turbine Design and Analysis System (TDAAS), each with a different eddy-viscosity RANS based turbulence model with transition capability. Experiments were conducted in a low speed wind tunnel to provide transition models for computational comparisons. The Reynolds number range based on axial chord and inlet velocity was $20{,}000 < Re < 100{,}000$ with an inlet turbulence intensity of 3.1%. Predictions using TDAAS agreed well with the measured Reynolds lapse rate. Computations using Fluent however, predicted stall to occur at significantly higher Reynolds numbers as compared to experiment. Based on triple sensor hot-film measurements, Fluent‟s premature stall behavior is likely the result of the eddy-viscosity hypothesis inadequately capturing anisotropic freestream turbulence effects. Furthermore, rapid distortion theory is considered as a possible analytical tool for studying freestream turbulence that influences transition near the suction surface of LPT airfoils. Comparisons with triple sensor hot-film measurements indicate that the technique is promising but more research is required to confirm its utility.

INTRODUCTION

Understanding low pressure turbine (LPT) Reynolds number effects is important for engines which must operate at high altitudes, and also for engines with LPT airfoils with very high aerodynamic loading. High-flying aircraft such as unmanned aerial vehicles (UAVs) experience large Reynolds number variation between take-off and cruise conditions. At low Reynolds numbers, which occur at high altitude, the boundary layers contain less energy and thicken, thereby making them more susceptible to separation when subjected to adverse pressure gradients. Although turbines operate with an overall favorable pressure gradient, the suction surface curvature causes localized regions of adverse pressure gradient, which can cause boundary layer separation and increased losses at low Reynolds numbers in LPTs. The loss or efficiency plotted against the Reynolds number is commonly called the Reynolds lapse.

Increasing the aerodynamic load on airfoils is desirable to reduce airfoil count and LPT weight. For given gas angles (constant work coefficient), increasing the aerodynamic load not only results in increased pitchwise spacing, but also in more highly curved airfoils. Increased curvature on the suction surface has potential to strengthen local adverse pressure gradients and cause separation at higher Reynolds numbers as compared to airfoils with reduced loading. The Zweifel loading coefficient, Z_w, is typically used to describe aerodynamic loading and is historically of the order of 1.0 [1]. Recent studies in the literature have focused on much higher loading levels. For example, Praisner et al. [2] investigated the loss behavior for airfoils with $1.15 < Z_w < 1.8$ with the aim of reducing airfoil count. Furthermore, low Reynolds number performance is also strongly dependent on the pressure coefficient profiles.

This paper focuses on the computational challenges of predicting midspan low Reynolds number performance. The airfoils used in the study are discussed first, followed by the transition models employed. Computational methods are presented next, followed by a discussion of the experimental arrangement and instrumentation for providing benchmark transition models. The results are then presented, which focus on the predictive quality of the transition models, and the interpretation of the results relative to the way the transition models were developed and calibrated. Finally, rapid distortion theory is discussed as a possible analytical technique to study turbulence effects that eddy viscosity models fail to capture.

AIRFOIL DEVELOPMENT

Recently, the Propulsion Directorate of AFRL developed a series of low pressure turbine airfoils for studying low Reynolds number, high-lift aerodynamics. These airfoils were designed in keeping with the Pratt & Whitney Pack B gas angles. The first pair of blades, L1M and L1A, were designed with incompressible Zweifel coefficients 17% greater than Pack B (i.e., Z_w=1.34 for L1M and L1A, Z_w = 1.15 for Pack B) and both mid- and aft-loaded pressure distributions, respectively. The L1M (level one increase in lift, mid-loaded), was first tested and analyzed outside of AFRL by Bons et al. [3] experimentally, and computationally by Gross and Fasel [4]. The airfoil was shown to have a significantly better Reynolds-lapse characteristic than the Pack B airfoil. The L1A (aft-loaded) airfoil was designed to the same level of loading as L1M, but it had too high a degradation in performance at low Reynolds numbers to make it more suitable for flow control studies under the NASA Fundamental Aeronautics Program [5, 6]. Subsequently, both airfoils were used in an investigation of the aerodynamic challenges in the operation of variable-speed power turbines for rotor-craft applications [7].

More recently another pair of cascade airfoils with incompressible Zweifel coefficients of 1.59 was designed to the Pack B gas angles. Again, the airfoils differed with respect to their loading conventions. The first one, designed by McQuilling [8], was front-loaded (L2F) whereas the second one that appears for the first time here, is more aft-loaded (L2A). This pair of airfoils was designed to test the limits of high lift, low Reynolds-number operation enabled by increases in the fidelity of CFD transition modeling. Both airfoils were predicted to have better Reynolds-lapse characteristics than the P&W Pack B despite increases in loading that were of order 38% over that high-lift airfoil.

Like the L1A and L1M, the AFRL L2-series of high-lift airfoils were designed using in-house analysis tools (TDAAS) that include the profile generator of Huber [9]. That algorithm uses Bezier curves in conjunction with typical leading- and trailing-edge specifications (e.g., wedge angles, edge radii of curvature, gage areas, and uncovered turning) to define airfoil shapes using a small number of control points in keeping with the method described by Casey [10]. Once the profile was defined, the grid generator and RANS solver described by Dorney and Davis [11] were used along with an ad hoc implementation of the transition models of Praisner and Clark [12] to determine airfoil performance. Graphical User Interfaces (GUIs) and both design optimization [13] and design-of-experiments techniques [14] were used during the design process to define the shape of the profiles.

DISCUSSION OF TRANSITION MODELS

Both codes used in the present study, TDAAS and Fluent, utilized transition models for low Reynolds number calculations. Walters and Leylek [15, 16] developed the transition model implemented in Fluent, which is the k-k_l-ω three-equation model, designed for modeling both natural and bypass transition. In natural transition, laminar boundary layers grow, eventually becoming unstable with the formation of Tollmien-Schlichting waves. As the flow continues, the Tollmein-Schlichting waves break down, forming turbulent spots, which are followed by a fully turbulent boundary layer. In bypass transition, freestream turbulence causes the natural process to be bypassed. (Schlichting and Gersten [17] discuss both types of transition.) The three transport equations in Fluent are used to solve for the turbulent kinetic energy, k, the laminar kinetic energy, k_l, and the specific dissipation, ω. Walters and Leylek [15, 16] added the transport equation for k_l to model streamwise laminar fluctuations in a pre-transitional boundary layer that eventually transitions to a turbulent boundary layer. After transition initiates, k_l is transferred to k to model the transition to full turbulence.

The k-k_l-ω model in Fluent was originally proposed as k-k_l-ε [15], where ε is the farfield turbulence dissipation rate. The authors then recast the transport equation for ε in terms of ω [16]. The model constants were determined from direct numerical simulations of fully turbulent channel flow and flat plate boundary layer experiments [16]. The latter model [16] is commercially available in Fluent and was used in the present study.

Because the Fluent k-k_l-ω model is recent, there are few studies in the literature using it. Sanders et al. [18, 19] reported that the model is a more accurate predictive tool for LPT airfoils as compared to conventional RANS based models. Cutrone et al. [20] compared the predictive quality of the k-k_l-ω model with five other transition models, all derived by combining a transition onset correlation with an intermittency factor based transition model to model the transition length. Cutrone et al. [20] concluded that the k-k_l-ω model performed best in all cases, except a flat plate case that had a strong pressure gradient in the transition region.

The separated flow transition model of Praisner and Clark [12] was employed in TDAAS for the present study. This model utilizes a single correlation from experiments to predict the turbulent reattachment point of a laminar separation bubble. The transition model is coupled with the Baldwin-Lomax [21] algebraic turbulence model to close the RANS equations. The model was derived from 47 experimental test cases for separated flow transition. Using dimensional analysis, Praisner and Clark [12] found that the separation bubble length correlated well according to Eq. (1),

$$\frac{B}{SS_{sep}} = 173.0 \mathrm{Re}_{\theta,sep}^{-1.227} \tag{1}$$

where B is the distance from separation onset to turbulent reattachment (bubble length), $\mathrm{Re}_{\theta,sep}$ is the momentum thickness Reynolds number at separation onset, and SS_{sep} is the suction surface distance from the leading edge to the separation point. The predictions presented in this paper did not utilize Praisner and Clark‟s [12] attached flow transition model. It is believed that using only the separated flow model is more conservative, since depending on the turbulence level, transition may occur in the experiment upstream of separation.

Praisner et al. [22] presented experimental validation data for the attached and separated flow models. The models accurately predicted the Reynolds lapse at midspan for the pack B profile, based on cascade experiments of Bons et al. [23]. Multistage 3D simulations were compared with experimental data from Binder et al. [24]. Where the flow was primarily two-dimensional, efficiency predictions using the attached and separated flow transition models agreed well with experiment, outperforming fully turbulent predictions, which underpredicted the efficiency between 1% and 2%. Transition modeling did not improve agreement in the endwall regions. Schmitz et al. [25] applied the Praisner and Clark [12] separated flow transition model for designing a research LPT stage, which was tested in a high-speed rotating rig. Total pressure loss predictions were performed as low as Re = 20,000, indicating stall-free operation for all Reynolds numbers examined. The researchers operated the rig as low as Re = 14,000 (based on inlet velocity and true chord), without observing separation. Again however, spanwise efficiency predictions were poor in the endwall region. With or without transition modeling, RANS-based turbulence models predict total pressure loss and efficiency poorly in the endwall region.

COMPUTATIONAL METHODS

The authors provide computational predictions using both the commercial code Fluent, and AFRL‟s TDAAS system. The computational procedures were quite different for the two codes. In Fluent, the pressure-based solver was used for all calculations due to low Mach numbers in the experiment ($M_{ex} <$ 0.06). The RANS equations were closed using the k-k_l-ω transition model [16]. Second order accurate finite volume spatial discretization was utilized. For time integration, either steady or unsteady formulations were used, depending on the Reynolds number. In general, the steady solver was used for high Reynolds numbers. At low Reynolds numbers, solutions usually failed to converge using the steady solver, which was evident by the lift coefficient and scaled residuals not reaching steady state. In that case, unsteady solutions were computed with an implicit, dual time-stepping formulation with second order accuracy. Solutions were assumed converged when the lift coefficient became steady periodic, indicating that all effects of initialization had decayed.

The domain modeled in Fluent was based on a single airfoil, with the inlet extending an axial chord upstream of the leading edge. The outlet was placed two axial chords downstream of the trailing edge. Periodic boundaries were assigned mid-pitch from the pressure and suction surfaces to model a single blade passage. The calculations were carried out using two dimensional, multi-block hybrid grids. A structured block with an O-type topology was used for discretizing the boundary layer around the airfoil surface, while an unstructured block was used for discretizing the remainder of the domain. Refining the grid to approximately 60,000 cells gave grid-independent results. In addition, boundary layers were sufficiently refined, with y^+ levels less than unity along the wall.

McQuilling [8] provides a detailed discussion of the computational procedures using TDAAS. Relevant details of the solver, grids and calculation procedure are discussed here for convenience. The grid generator and flow solver is that described by Dorney and Davis [11]. The solver is density-based and is used to solve the RANS equations using an implicit dual time stepping, time-accurate approach. The time integration scheme is second order accurate, with convergence being obtained when the pressure field downstream of the trailing edge becomes steady periodic. The spatial discretization is based on a third order accurate, finite difference upwinding scheme. Since the Dorney and Davis [11] flow solver was not preconditioned to handle low Mach number flows, the exit Mach number was set at M_{ex} = 0.2 to reduce the stiffness of the governing equations while maintaining incompressible flow. Reynolds numbers were matched by reducing the fluid density.

Due to using finite differencing, the solver in TDAAS required structured grids. The grids were based on a multi-block O-H topology. The O-type mesh was used for discretizing the boundary layer, with H-type meshing used for the remainder of the domain. Due to higher order finite differencing and structured meshing, grid independent results were achieved with approximately 7,000 grid points for the 2D passage. Furthermore, y^+ levels along the wall were less than unity.

Implementation of the Praisner and Clark [12] separated flow transition model in TDAAS requires a two-step procedure. A converged fully laminar solution is computed first to obtain $\mathrm{Re}_{\theta,sep}$ and SS_{sep} as inputs for Eq. (1). After using Eq. (1) to define the reattachment point, the turbulent wall boundary layer downstream of the separation bubble is computed using the Baldwin-Lomax algebraic model [21]. Note that for reattachment points predicted beyond the trailing edge, only the laminar solution is utilized, resulting in outright separation. For more information regarding implementation, the reader is referred to Praisner and Clark [12].

EXPERIMENTAL METHODS

The experiments were conducted using the AFRL low speed wind tunnel facility. This wind tunnel is an open loop induction type, with the flow entering a bell-mouth contraction and passing through a turbulence-generating grid. The turbulence grid is comprised of a lattice of horizontal and vertical 25.4 mm round bars, with 76.2 mm center spacing. The center blade of the cascade is approximately 90 bar diameters downstream of the grid. The turbulence grid produces a turbulence intensity of Tu = 3.1%, with an integral scale of L_{in} = 39.2 mm at about 1.4C_{ax} upstream of the cascade. Aft of the cascade, the flow passes through the exit duct to enter the fan.

A schematic of the test section is given in Fig. 1. As shown, the cascade is comprised of seven airfoils. The end-flow adjusters were used to control the bypass flow around the outside of the cascade to achieve periodicity. A single outer tailboard was used to set the exit angle at Re = 100k. The authors acknowledge that the exit angle will change as Re decreases, approaching stall. Exit traverse data were collected at midspan, 0.75C_{ax} downstream of the cascade in the axial direction. The traverse plane origin is defined downstream of the middle blade as the intersection of the tangent line projected from the pressure side of the trailing edge, and the traverse plane. The tangent line projected from the pressure side of the trailing edge originates from the intersection of the trailing edge circle and the pressure surface. An additional traverse plane is defined inside a single passage at midspan, at 0.5C_{ax}. The origin of this traverse plane is defined at the blade suction surface. The same cascade definitions are used for both airfoils in the present study, the L2A and L2F. Table 1 summarizes the relevant geometric data and flow conditions. The flow angles are design point values.

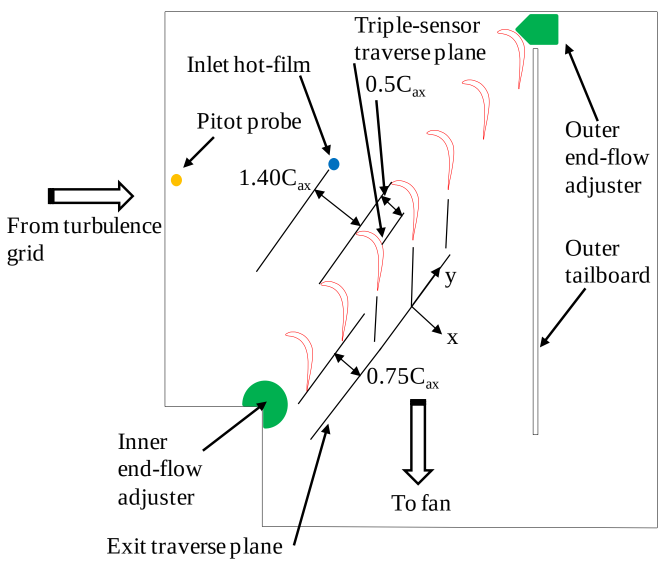

Figure 1. Schematic of AFRL low speed wind tunnel test section.

An upstream stationary pitot probe and a kiel probe in the exit traverse plane were used to measure total pressure loss. At 3.2 mm, the kiel probe diameter was less than 2% of the blade pitch, providing sufficient resolution within the wakes. The ambient pressure was measured with a laboratory barometer and freestream fluid temperatures were measured using type J thermocouples. An IFA300 constant temperature anemometer was used with single normal hot-film probes (TSI 1211-20) for obtaining velocities, turbulence intensities, and integral length scales at the inlet, and exit traverse. A TSI 1299-20-18 triple sensor hot-film probe was used to obtain freestream turbulence measurements within the triple sensor traverse plane (Fig. 1), but only for the L2A cascade. All three sensors of the triple probe were contained in a 2 mm measurement diameter. The probe stem however, was 4.6 mm in diameter.

Table 1. Cascade Geometry and Flow Conditions

Axial chord, C_{ax}	152.4 mm
Pitch/axial chord, P/C_{ax}	1.221
Span/axial chord, H/C_{ax}	5.75
Zweifel coefficient, Z_w	1.59
Inlet flow angle, α_{in}	35
Exit flow angle, α_{ex}	58
Inlet turbulence Intensity, Tu_{in}	3.1%
Streamwise integral scale at inlet, L_{in}	39.2 mm
Max exit Mach number, M_{ex}	0.053

All hot-film probes were calibrated using a TSI Model 1127 velocity calibrator. Typical calibration curves included 18 points, spanning the measured velocity range in the experiment. Table 2 displays the calibration velocity ranges for the probes. During calibration, the triple sensor probe was placed in a zero pitch/yaw configuration for the entire velocity range. An analytical technique, similar to that described by Lekakis et al. [26] was used to obtain the velocity angles and magnitudes in the experiment, given effective cooling velocities from the three sensors. In the experiment, flow angles relative to the probe axis were small, at less than 6. Angle measurements on the calibration stand however, were within 0.5 of the actual velocity vector for 12 pitch and yaw.

Table 2. Calibration velocity ranges for hot-film probes.

Probe	Min Velocity, m/s	Max Velocity, m/s
Inlet film	1.5	11.5
Exit film	10	18.5
Triple-film	5	29

Besides ambient pressures, all other data were sampled using National Instruments hardware and software. When capturing data used for computing the integral scales, the analog signal was conditioned with a low pass filter at a 5 kHz cutoff frequency. The analog signal was sampled at 20 kHz, well above the Nyquist criterion to prevent aliasing. The integral length scales were computed by first calculating the autocorrelation function, as given by Eq. (2).

$$R_{xx}(s) = \frac{\int_0^T u(t)u(t+s)dt}{\int_0^T u(t)u(t)dt} \qquad (2)$$

The integral time scale, τ, was then taken as the value of *s* such that $R_{xx}(s) = 1/e$, as proposed by Tritton [27]. The integral length scales were then computed for the streamwise direction by invoking the frozen turbulence approximation and multiplying τ by the mean velocity.

All uncertainties were calculated at 95% confidence. Uncertainties for the Reynolds number and total pressure loss coefficients were estimated using the partial derivative and root-sum-square method of Kline and McClintock [28]. The uncertainty of the peak loss coefficients and Reynolds numbers were less than 5% and 3.5%, respectively, of the measured values over the entire Reynolds number range. Hot-film velocity measurements were the largest source of uncertainty.

The uncertainty of the turbulence measurements downstream of the cascade was estimated by constructing confidence intervals for ensembles of 25 data sets for each measurement location. Within the wakes, the precision error of the integral scales was within 5% of the measured values. In the freestream between the wakes, the precision error was larger, but typically within 10% of the measured values. (Roach [29] reported that uncertainties in calculating integral scales can easily reach 10%.) The precision uncertainty for the turbulence intensity was lower, at less than 3% of the mean measured value. Upstream of the cascade, sufficient data were captured to reduce the precision uncertainty of the inlet integral scale and turbulence intensity to less than 2% of the mean values. Precision error also dominated for the triple sensor measurements. Mean square velocity fluctuations were within 10% of the measured values for the triple sensor probe.

RESULTS AND DISCUSSION

In this section of the paper, comparisons between computational and experimental data are presented and discussed in terms of predictive quality. Discrepancies between predictions and experiments are then discussed relative to the way the transition models emulate the flow physics.

Reynolds Lapse Predictions

It is imperative that the designer has confidence in the general trend of the predicted lapse curve. Said another way, it is necessary to know whether the boundary layer will separate, transition, and re-attach with only a modest increase in loss with decreasing Reynolds number, or whether the viscous layer separates without re-attachment. If the latter prevails, then the designer needs to know the Reynolds number at which this occurs.

The Reynolds lapse for the front-loaded L2F airfoil is presented in Fig. 2. As shown, the losses for this airfoil increase modestly with decreasing Reynolds number as compared to the Pack B. This result, first observed by McQuilling [8] is significant, considering that the Pack B and L2F were designed with $Z_w = 1.15$ and $Z_w = 1.59$, respectively. McQuilling [8] also presented detailed suction surface boundary layer measurements for L2F. Based on shear stress measurements, McQuilling [8] showed that a separation bubble is present on the airfoil in the range of 25k < Re < 75k. McQuilling [8] also presented hotwire measurements down to 1 mm from the suction surface without observing reversed flow, indicating an extremely thin separation bubble. The Reynolds number at separation onset is unknown for L2F.

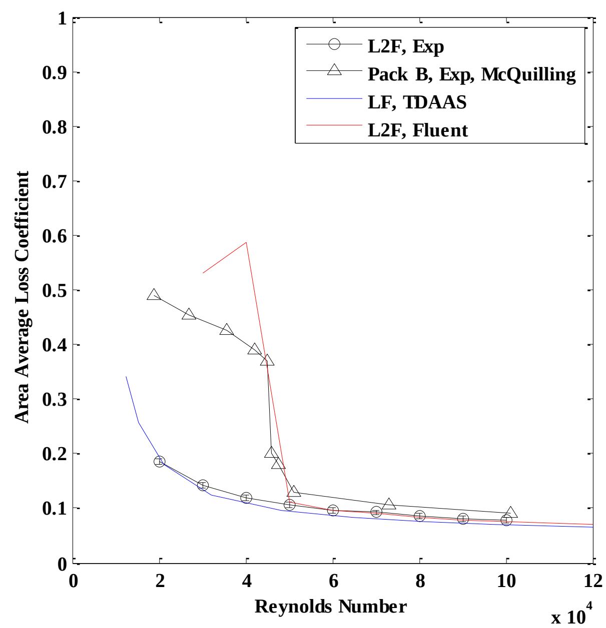

Figure 2. Experimental and computational Reynolds lapse for L2F. The Pack B results are from McQuilling [8].

Predictions for L2F using TDAAS agree well with the measurements across the entire Reynolds number range, being only slightly below the error bars. The calculations using Fluent however, predicted L2F to stall below Re = 50k, similar to Pack B. Before stall occurs, the Fluent predictions are quite accurate and within experimental uncertainty. Fluent predictions were not computed at lower Reynolds numbers because they were considered unnecessary after determining the stall location.

Figure 3 presents the Reynolds lapse for the L2A airfoil. Unlike L2F, the measurements indicated stall below Re = 40k, which is still a slight improvement over Pack B. At present, no suction surface boundary layer measurements are available for L2A. Overall, lapse predictions using TDAAS follow the trend quite well, but under-predict the loss magnitude within the range of 40k < Re < 90k. The TDAAS calculations also reasonably predict the Reynolds number at which stall occurs. The Fluent calculations predict earlier stall at nearly twice the Reynolds number of the measured stall location. Similar to L2F, the Fluent loss predictions for L2A are quite accurate and within experimental uncertainty before the airfoil stalls.

Additionally, neither code agrees well with the measured losses once stall occurs.

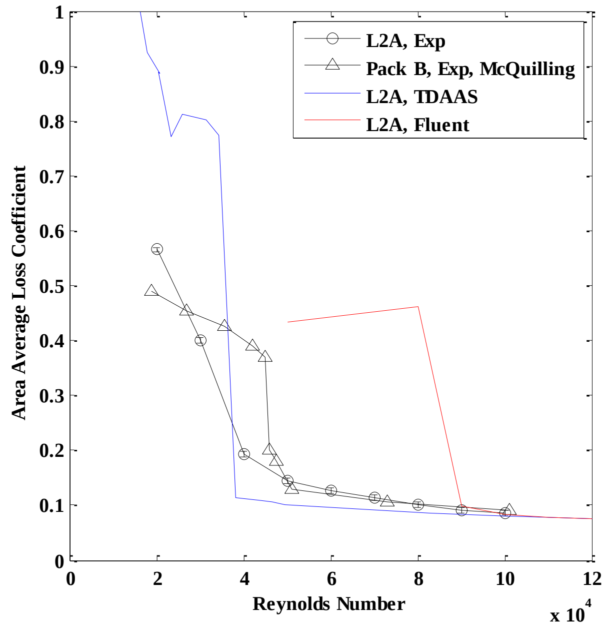

Figure 3. Experimental and computational Reynolds lapse for L2A. The Pack B results are from McQuilling [8].

The differences in the Reynolds lapse for the L2A and L2F airfoils are best explained by examining the pressure loading distributions. Figure 4 shows the pressure coefficients for both airfoils at midspan. These data were obtained computationally using Fluent‟s implementation of Shih et al.‟s [30] realizable k-ε turbulence model. The fully turbulent computations eliminated separation bubbles present on the suction surface to provide cleaner plots for illustrative purposes. Inviscid calculations using the Navier-Stokes grids had instabilities near the trailing edge and were not used. As shown, the loading is significantly different for the two airfoils. Peak loading for L2F and L2A occur at 25% and 60% axial chord, respectively. Because of front loading, the diffusion length on the suction surface of L2F is nearly 1.9X longer than L2A‟s diffusion length. As a result, the adverse pressure gradient is more severe for L2A, resulting in stall at higher Reynolds numbers. The improved stall performance of L2F however, does not make it an obvious design choice over L2A. Front loaded airfoil performance is much more sensitive to small changes in geometry [1], and generally result in higher endwall losses [31]. These factors must be considered during design.

It is easier to understand the differences in measured airfoil performance than the differences in computational predictions. As described above, the two transition models used in the present study were developed using very different design philosophies. The transition model implemented in TDAAS is correlation based, and was calibrated using a database of cascade results, comprised of both compressors and turbines. This model yielded superior stall predictions because it was developed using flows with high streamline curvature and straining, similar to the flows being studied. Because this model requires a previously converged laminar solution before implementing the turbulent solution, users may consider its use cumbersome.

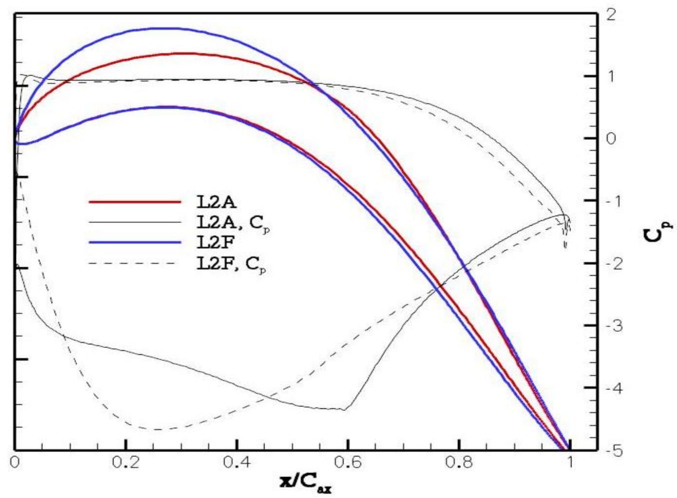

Figure 4. Pressure loading distributions for the L2A and L2F airfoils.

The k-k_l-ω model, which is available in Fluent, requires only a turbulent integral scale and intensity as boundary conditions, similar to fully turbulent RANS based, eddy viscosity turbulence models. The high loading levels present for the L2A and L2F airfoils were challenging for this model, which predicted stall prematurely for both airfoils. The model constants were calibrated with fully turbulent channel flow and flat plate boundary layer experiments [16], which may not accurately model the turbulence development when the flow is highly strained.

Furthermore, it is important to consider the methods for determining the turbulent boundary conditions implemented in Fluent to give confidence that they were not the cause of premature stall. The inlet turbulence intensity was determined to be 3.1% ± 0.062% at 95% confidence (2% of mean measured value). Since the turbulence intensity is obtained with straightforward statistical calculations, this result is believed to be a unique and valid inlet boundary condition. On the other hand, various methods exist for computing the turbulent integral scale, implying that the measured integral scale in the present study is not unique.

Sanders et al. [18] however, performed a parameter study using Fluent‟s version of the k-k_l-ω model to investigate the effect of inlet turbulence integral scale on the maximum wake loss coefficient of a cascade of LPT airfoils. The LPT airfoils modeled in their study were designed for use in the same experimental facility described in this paper, but with lower loading (Z_w = 0.94, C_{ax} = 177.8 mm). Sanders et al. [18] found that for L_{in} > 14 mm, the results were insensitive to the integral scale. Since the measured integral scale in the present study is L_{in} = 39.2 mm, a 10% variation due to a difference in calculation procedures as suggested by Roach [29], is not expected to influence the present results. Differences between the predictions and measurements are therefore attributed to the way the flow physics are modeled. The next section of the paper explores this topic.

Reasons for k-k_l-ω Stall Behavior

This section of the paper presents midspan turbulence measurements inside a single passage of the L2A cascade (see Fig. 1). It is well known that a turbulent boundary layer can overcome adverse pressure gradients better than laminar boundary layers. If a turbulence model fails to capture all the relevant freestream turbulence effects near the suction surface of an LPT airfoil, bypass transition can be delayed, causing stall prematurely.

The turbulent kinetic energy development at $0.5C_{ax}$ for the L2A cascade is given in Fig. 5. As shown, the predicted and measured turbulence development is qualitatively different. The measured turbulence energy decreases towards the wall, whereas the predicted turbulence energy increases. Also observe for the predicted turbulence development, that the kinetic energy goes to zero inside the boundary layer. It is interesting that Fluent predicted stall prematurely, even with computed turbulence energy levels more than 20% higher than the measured values in the freestream near the edge of the boundary layer. The measured Reynolds stresses give additional insight into the discrepancy.

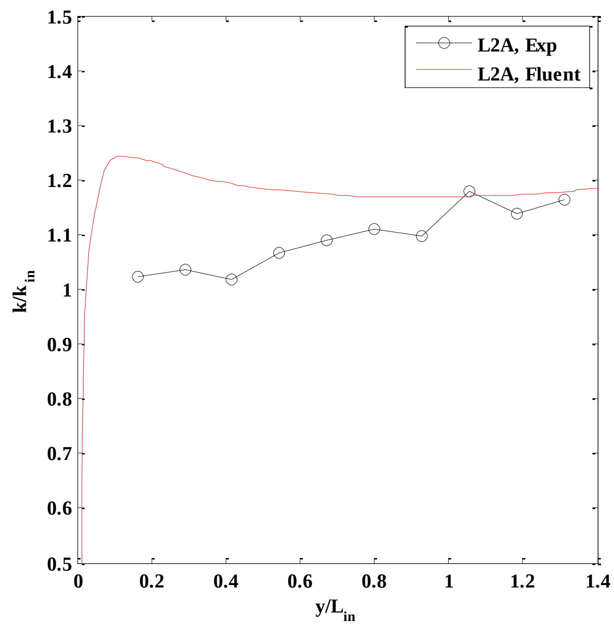

Figure 5. Turbulent kinetic energy at $0.5C_{ax}$ for the L2A cascade, normalized by the inlet turbulent kinetic energy. Re = 100k.

Figure 6 shows the measured components of the Reynolds stress tensor across the passage at $0.5C_{ax}$. These triple sensor results are presented in streamline coordinates. Therefore, u-fluctuations are in-line with the mean velocity vector, and the v and w-fluctuations are orthogonal to the mean velocity vector with zero mean velocity. Furthermore as the probe position approaches the wall, the v-velocity fluctuations become closer to the wall-normal direction. Because the turbulence entering the cascade was generated using a square lattice grid and was in the latter stages of decay (Tu = 3.1%), the turbulence is nearly isotropic, as described by Roach [29]. As shown in Fig. 6 however, the effect of high strain rates to accelerate the flow over the suction surface, and also the effect of streamline curvature has a dramatic effect on the incoming turbulence. Recall from Fig. 5 that the measured overall turbulent kinetic energy close to the wall is nearly the same value as the incoming turbulence. The turbulence energy is therefore redistributed directionally. The spanwise fluctuation component, $\langle w^2 \rangle$, is amplified close to the wall. The $\langle u^2 \rangle$ component gradually increases approaching the wall, whereas $\langle v^2 \rangle$ is damped.

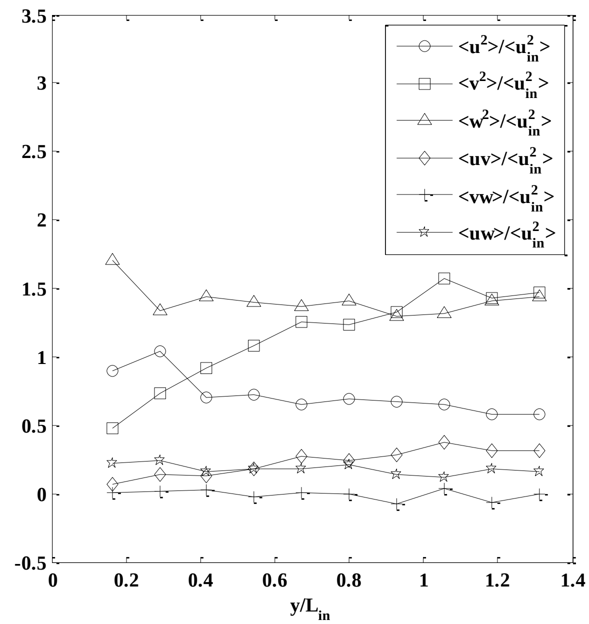

Figure 6. Measured components of the Reynolds stress tensor within the passage at $0.5C_{ax}$ for the L2A cascade. Re = 100k.

The Reynolds shear stresses are most interesting in Fig. 6. As shown, the $\langle uv \rangle$ and $\langle uw \rangle$ components are positive across the measurement range. The $\langle vw \rangle$ term is near zero, indicating negligible correlation between the two fluctuation components. The $\langle uv \rangle$ component decreases across the passage approaching the wall, whereas $\langle uw \rangle$ increases. The increasing $\langle uw \rangle$ term approaching the wall is a very interesting result. Since the measurements were taken at midspan of the passage, the RANS x-momentum equation indicates a negligible effect on the mean flow due to $\langle uw \rangle$, based on symmetry. Furthermore, the z-direction momentum equation simply becomes a balance in shear stress gradients at midspan. The $\langle uw \rangle$ term does not appear in the y-momentum equation. Although $\langle uw \rangle$ does not have an apparent effect on the mean flow, it may actually be an instability mechanism. If <uw> remains significant approaching the wall, it may interact with streamlines in the edge of the developing boundary layer. Considering that <uw> indicates a correlation between the streamwise, and dominant spanwise fluctuation components, its effect may be to buckle the streamlines and influence transition. This mechanism occurs in the x-z plane as opposed to instabilities in the x-y plane, possibly influencing both attached and separated flow transition processes.

The primary implication for turbulence modeling is that <uw> is zero by definition according to the eddy-viscosity hypothesis for two-dimensional flows. Any significant effect of <uw> in the experiment was not captured using Fluent. Wilcox [32] points out that the eddy-viscosity hypothesis fails for flows with high streamline curvature and extra rates of strain, both of which are present for high lift LPT flows. Researchers typically apply corrections to turbulence models to improve performance for challenging flows. The freestream turbulence measurements presented in this paper provide a possible explanation for the k-k_l-ω model‟s poor performance in predicting the Reynolds lapse, primarily due to a failure in the eddy-viscosity hypothesis. Because the TDAAS predictions were based on empirical modeling for similar cascade flows, all the anisotropic turbulence effects were captured implicitly. This is why TDAAS predicted stall more accurately than the Fluent predictions using the k-k_l-ω model.

As a consequence of high strain rates near the suction surface of LPT airfoils, rapid distortion theory may provide a means outside of DNS and LES to gain insight into the freestream turbulence field that interacts with the developing boundary layer. The purpose is to examine an alternative technique that does not require supercomputing facilities to study freestream turbulence effects. Improved knowledge of the freestream turbulence field can be used to apply corrections to eddy viscosity based transition models. The next section of this paper investigates this possibility.

Freestream Turbulence and Rapid Distortion Theory

Governing equations for the fluctuating velocity components in a turbulence field are obtained by subtracting the RANS from the Navier-Stokes equations. Pope [33] presents these equations in incompressible form while neglecting the energy equation as,

$$\frac{Du_j}{Dt} = -u_i\frac{\partial\langle U_j\rangle}{\partial x_i} - u_i\frac{\partial u_j}{\partial x_i} + \upsilon\nabla^2 u_j - \frac{1}{\rho}\frac{\partial p}{\partial x_j} \tag{3}$$

and

$$\frac{1}{\rho}\nabla^2 p = -2\frac{\partial\langle U_i\rangle}{\partial x_j}\frac{\partial u_j}{\partial x_i} - \frac{\partial^2 u_i u_j}{\partial x_i \partial x_j}, \tag{4}$$

where the bracketed and lower case terms are mean, and fluctuating quantities, respectively. Note that the *i* and *j* indices represent three space dimensions in a Cartesian coordinate system. Only the mean velocity gradients appear and not the mean velocity. These mean velocity gradients are taken to be known, and can be time dependent. The idea with rapid distortion theory is that if the turbulence field is subjected to large strain rates, the linear terms containing the mean velocity gradients will dominate over the turbulence-turbulence interaction terms. Therefore, the second and third terms on the right hand side of Eq. (3), along with the second term on the right hand side of Eq. (4) can be neglected, resulting in linear equations which are more easily solved. In their linear form, the governing equations for the fluctuating velocity and pressure are called the rapid distortion equations.

It is important to first assess whether or not rapid distortion theory applies to LPT flows. Hunt and Carruthers [34] provide the essential criterion for rapid distortion theory to apply in terms of turbulent scales. This criterion is given by Eq. (5),

$$\frac{\sqrt{< u^2 >}}{L}\left(\frac{l}{L}\right)^{-\frac{2}{3}} << \max\left(\frac{\Delta\langle U\rangle}{d}, \frac{1}{T_D}\right) \tag{5}$$

where l is a turbulent scale to be evaluated, L is the turbulent integral scale, d is the distance along which the distortion occurs, and T_D is the time required for the distortion to occur. Equation (5) indicates that rapid distortion theory is most applicable for large turbulent scales.

Assuming that the energy containing eddies occur for scales in the range of 1/6L < l < L [33], the right hand side of Eq. (5) was approximated to be between 4X and 13X larger than the left hand side for the L2-series airfoils. To calculate the ratio, mean velocities were extracted from computational results approximately a half axial chord upstream of the leading edge, and at mid-axial chord, just outside of the boundary layer in the freestream. Because the inlet integral scale and turbulence intensity are insensitive to the Reynolds number for grid generated turbulence [29], taking the ratio of the right to left hand sides of Eq. (5) is also expected to be insensitive to the Reynolds number. Therefore, Eq. (5) is expected to apply over the experimental Reynolds number range.

Figure 7 is a contour plot of velocity magnitude, scaled by the inlet velocity, to give insight into the parts of the flow domain where rapid distortion theory may apply. As shown, the highest velocities will occur within the freestream, close to the suction surface. The boxed region in the figure indicates the high strain region. Furthermore, a fluid particle in the freestream passing over the suction surface must double its velocity in a distance shorter than an axial chord. Hence, rapid distortion theory is expected to be most applicable in that part of the flow. Additionally, it is flow along the suction surface that will interact with a developing boundary layer, influencing turbulent transition. Flow acceleration is less severe near the pressure side of the passage, suggesting that rapid distortion theory does not apply in that part of the flow.

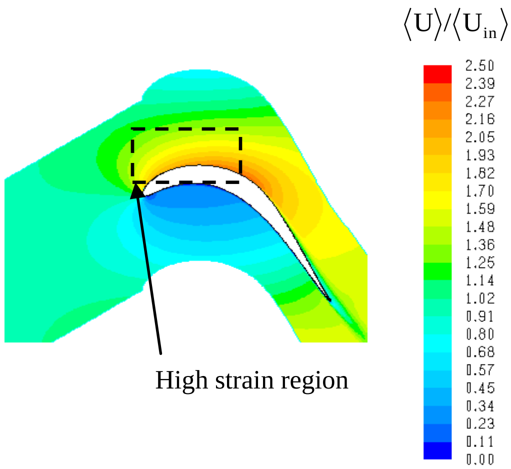

Figure 7. Contour plot of the scaled velocity magnitude for the L2A airfoil.

Whether or not a rapid distortion event has occurred can also be determined by examining the turbulent integral scales downstream of the distortion. Hunt and Carruthers [34] claim that for rapidly distorted, inhomogeneous turbulence near a rigid surface, with or without mean shear, the two-point spatial correlations of the turbulence field change little during the distortion. Hence, the integral scales which are obtained from two-point spatial correlations are also expected to change little near a rigid boundary, similar to the suction surface of high lift LPT airfoils. Therefore, the size of the turbulent eddies that pass through the high strain region of the freestream near the airfoil suction surface is expected to remain approximately constant.

To investigate the effect of the airfoils on the integral scales, integral length scale measurements were taken at the exit traverse plane, and normalized by the measured values taken at the cascade inlet. These measurements are presented in Fig. 8 along with total pressure loss coefficients to indicate the blade wakes. The subscript "loc" indicates a measurement in the exit traverse plane. The right side of the wakes corresponds to the suction side of the airfoils. If a rapid distortion event occurs, L_{loc}/L_{in} = 1.0 is the expected result. As shown, the normalized integral scales for both airfoils are near unity just outside of the wake on the suction side (y/Pitch $\cong$ -0.7). This result suggests that rapid distortion theory provides a reasonable description of turbulence development along the airfoil suction surface within the freestream. The integral scales decrease farther towards the airfoil pressure surface, followed by an abrupt increase as the freestream interacts with the shear layer from the blade pressure surface. The integral scales are smallest within the blade wakes, which are due to mixing within the wake and not from the incoming grid generated turbulence.

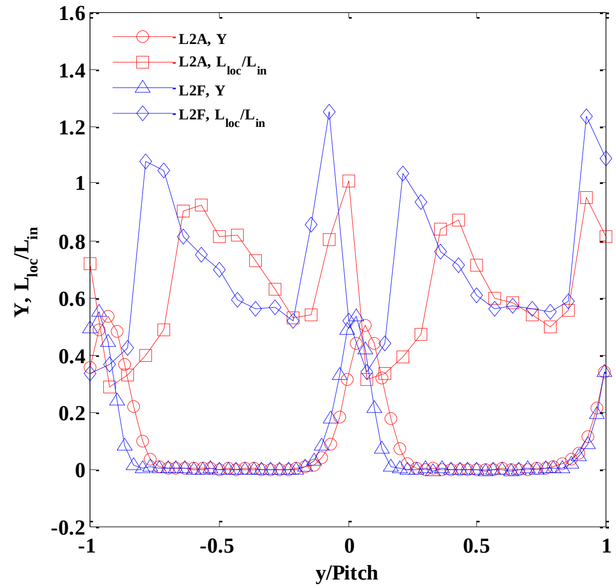

Figure 8. Pitchwise integral scale development in the exit traverse plane for the L2A and L2F airfoils. Data were captured at Re = 100k.

Considering that scaling arguments and integral scale measurements both indicate that rapid distortion may be present, we will now examine the turbulent kinetic energy development. Goldstein and Durbin [35] solved the rapid distortion equations for two-dimensional contractions with various incoming turbulence integral scales, and contraction ratios. The incoming turbulence was isotropic for all cases. Their geometry is sketched in Fig. 9, which consisted of a plane strain contraction. The important aspect of Goldstein and Durbin‟s [35] results was the effect of high strain on the turbulence approaching the wall, but outside the boundary layer. Goldstein and Durbin [35] presented their plane strain results for the normal Reynolds stresses in terms of the parameters δ_1/δ_2 and $2\delta_2/L_{in}$. Both of these parameters significantly influence turbulence amplification near the wall.

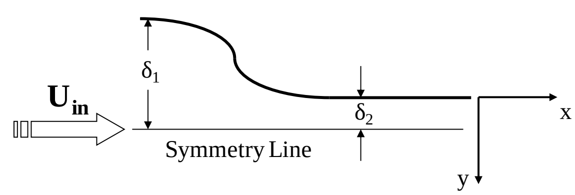

Figure 9. Sketch of Goldstein and Durbin‟s [35] geometry.

Figure 7 was used to obtain the required parameters for use with the Goldstein and Durbin [35] results. As shown, the space between the suction surface and the top of the high strain region in Fig. 7 was approximately $0.25C_{ax}$ and is taken to be the downstream contraction height, $2\delta_2$. Additionally, $0.25C_{ax} \cong L_{in}$, so the inlet integral scale is approximately equal to the downstream contraction height ($L_{in} \cong 2\delta_2$). As for contraction ratio, the fluid speed near the suction surface is approximately double the incoming fluid speed. This correlates by continuity to $\delta_1/\delta_2 = 2.0$. The parameters $\delta_1/\delta_2 = 2.0$ and $2\delta_2/L_{in} = 1.0$ were used as inputs in obtaining predictions using the Goldstein and Durbin [35] plane strain results.

The plane strain turbulence development is compared with the measured results from the L2A cascade in Fig. 10. Note that $<u^2>$ is for the streamwise direction, $<v^2>$ is for the wall-normal, or y-direction, and $<w^2>$ is for the spanwise direction (in and out of page for Fig. 9). Similar to the measurements, the predictions indicate highly anisotropic turbulence development due to large strain rates. The predicted spanwise fluctuation component, $<w^2>$, is clearly dominant, similar to experiment. The predicted turbulent kinetic energy increases approaching the wall, but remains near unity until $y/L_{in} < 0.1$. The measured $<v^2>$ component decays more rapidly approaching the wall than the predicted values for plane strain, indicating that the wall damping effect is more significant than rapid distortion theory suggests. The predicted streamwise component, $<u^2>$, is consistently less than the measured values.

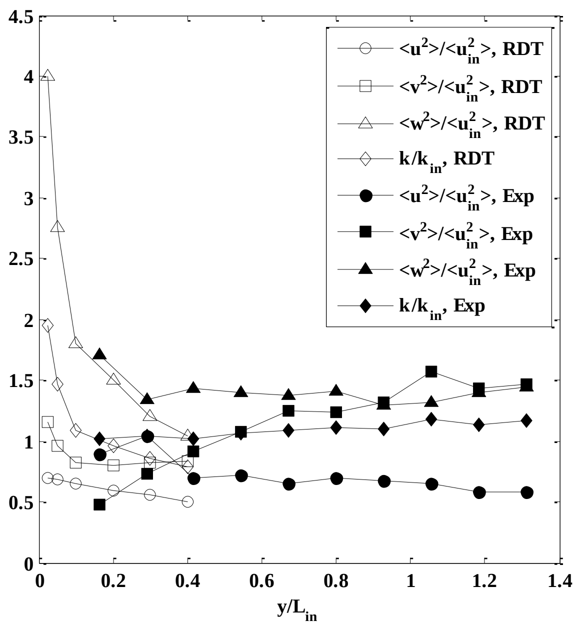

Figure 10. Comparison of L2A midspan turbulence development at $0.5C_{ax}$ with plane strain rapid distortion. Re = 100k for experimental results. ($\delta_1/\delta_2 = 2.0$ and $2\delta_2/L_{in} = 1.0$ for plane strain results of Goldstein and Durbin [35])

The results presented in Fig. 10 indicate that rapid distortion theory can capture the physical processes that redistribute the fluctuation energy. The magnitudes however, were clearly different. This result is not surprising considering that the rapid distortion predictions were based on a plane strain contraction. This flow is considerably different than the LPT airfoils. Furthermore, measurements could not be made any closer to the wall in the present study, due to concerns of probe interference with the flow and probe damage. Measurements are needed close to the wall, along with rapid distortion predictions for an equivalent flow to make a complete assessment of rapid distortion theory for this application. The idea is to find a tool to study turbulence development with less computational overhead than LES and DNS. These insights can be used to modify eddy-viscosity models to improve low Reynolds number performance.

CONCLUSIONS

The Reynolds lapse behavior for linear cascades of L2A and L2F airfoils was investigated experimentally and computationally. Experiments were conducted over a Reynolds number range of 20,000 < Re < 100,000 with an inlet turbulence intensity of 3.1% and a streamwise integral scale of 39.2 mm. The front-loaded L2F airfoil experienced only modest loss increases with decreasing Reynolds number, attributed mainly to a weak adverse pressure gradient on the suction surface. This airfoil did not stall. The aft-loaded L2A airfoil however, stalled catastrophically for Re < 40,000 as a result of a strong adverse pressure gradient on the suction surface.

Reynolds lapse predictions obtained using AFRL‟s TDAAS system, which included Praisner and Clark‟s [12] separated flow transition model, agreed well with experiments for both airfoils. Predictions using Fluent‟s implementation of the k-k_l-ω model [15, 16] however, were overly conservative, predicting stall prematurely for both airfoils, which was not observed during the experiments. For the L2A airfoil, the Fluent calculations predicted stall at nearly twice the experimental stall Reynolds number. The k-k_l-ω model‟s stall behavior is likely attributed to a failure in the eddy-viscosity hypothesis to fully resolve the anisotropic turbulence effects caused by high strain rates and turning. Specifically, a non-zero $<uw>$ Reynolds shear stress component was found in the experiment, which may act as an instability mechanism. The eddy viscosity hypothesis assigns $<uw> = 0$ by definition for a 2D flow. Because the transition model in TDAAS was empirically derived from similar flows, the freestream turbulence effects were captured implicitly, leading to improved results.

As a consequence of high strain rates near the suction surface of LPT airfoils, rapid distortion theory may provide a computationally less expensive tool compared to DNS and LES to gain insight into the freestream turbulence field that interacts with the developing boundary layer. The information gained can be used to apply corrections to low Reynolds number eddy viscosity transition models. The results in this paper indicate that the technique is promising, but more research is needed to confirm its utility.

NOMENCLATURE

B	separation bubble length
C_{ax}	axial chord
C_p	pressure coefficient, $C_p = \left(P_s - P_{s,in}\right)/0.5\rho\langle U_{in}\rangle^2$
d	distance over which a rapid distortion occurs
H	blade span
k	turbulent kinetic energy, $k = 0.5(<u^2> + <v^2> + <w^2>)$

k_l	laminar kinetic energy
M	Mach number
l	arbitrary turbulent scale
L	turbulence integral scale
p	fluctuating static pressure
P	blade pitch
P_s	static pressure
P_t	total pressure
RANS	Reynolds-averaged Navier-Stokes
Re	Reynolds number based on inlet velocity and axial chord
R_{xx}	autocorrelation function
SS	suction surface
t	time variable
T_D	time duration for a rapid distortion
Tu	turbulence intensity, $\sqrt{<u^2>}/\langle U\rangle \times 100\%$
U(t)	instantaneous velocity
$\langle U\rangle$	mean velocity
u(t)	velocity fluctuation, $u(t) = U(t) - \langle U\rangle$
$<u^2>$	x-direction mean square fluctuation
$<v^2>$	y-direction mean square fluctuation
$<w^2>$	z-direction mean square fluctuation
x	axial direction coordinate
y	pitchwise direction coordinate
Y	total pressure loss coefficient, $Y = \left(P_t - P_{t,in}\right)/0.5\rho\langle U_{in}\rangle^2$
Z_w	Zweifel loading coefficient, $Z_w = 2\left(\frac{P}{C_{ax}}\right)\cos^2\alpha_{ex}\left(\tan\alpha_{in} - \tan\alpha_{ex}\right)$

Greek

α	cascade gas angle
δ_1, δ_2	contraction heights
ε	turbulence dissipation rate
θ	momentum thickness
ρ	density
τ	turbulence integral time scale
υ	kinematic viscosity
ω	turbulence specific dissipation

Subscripts

ex	exit location
i,j,k	Cartesian indices, can be 1, 2, or 3
in	inlet location
loc	local location
sep	separation location

REFERENCES

[1] Wilson, D.G., and Korakianitis, T., 1998, "The Design of High-Efficiency Turbomachinery and Gas Turbines," 2nd Edition. Upper Saddle River, New Jersey: Prentice Hall Inc.

[2] Praisner, T.J., Grover, E.A., Knezevici, D.C., Popovic, I., Sjolander, S.A., Clark, J.P., and Sondergaard, R., 2008, "Toward the Expansion of Low-Pressure-Turbine Airfoil Design Space," ASME Paper GT2008-50898.

[3] Bons, J. P., Hansen, L. C., Clark, J. P., Koch, P. J., and Sondergaard, R., 2005, "Designing Low-Pressure Turbine Blades with Integrated Flow Control," ASME Paper No. GT2005-68962.

[4] Gross, A. and Fasel, H. F., 2007, "Investigation of Low Pressure Turbine Separation Control," AIAA Paper No. 2007-520.

[5] Bons, J. P., Reimann, D., and Bloxham, M., 2008, "Separated Flow Transition on an LP Turbine Blade with Pulsed Flow Control," ASME *J. of Turbomachinery*, Vol. 130, pp. 021014-1:02101-8.

[6] Volino, R. J., 2010, "Separated Flow Measurements on a Highly Loaded Low-Pressure Turbine Airfoil," ASME *J. of Turbomachinery*, Vol. 132, pp. 011007-1:011007-10.

[7] Welch, G. E., 2010, "Assessment of Aerodynamic Challenges of a Variable-Speed Power Turbine for Large Civil Tilt-Rotor Application," 66th Forum of the American Helicopter Society, Phoenix, AZ, 11-13 May.

[8] McQuilling, M., 2007. "Design and Validation of a High Lift Low-Pressure Turbine Blade," PhD Thesis, Wright State University, Dayton, OH.

[9] Clark, J. P., Koch, P. J., Ooten, M. K., Johnson, J. J., Dagg, J., McQuilling, M. W., Huber, F., and Johnson, P. D., 2009, "Design of Turbine Components to Answer Research Questions in Unsteady Aerodynamics and Heat Transfer," AFRL Report No. AFRL-RZ-WP-TR-2009-2180.

[10] Casey, M. V., 1994, "Computational Methods for Preliminary Design and Geometry Definition in Turbomachinery," in Turbomachinery Design Using CFD, AGARD Lecture Series 195, pp. 1-1:1-22.

[11] Dorney, D. J. and Davis, R. L., 1992, "Navier-Stokes Analysis of Turbine Blade Heat Transfer and Performance," ASME *J. of Turbomachinery*, Vol. 114, pp. 795-806.

[12] Praisner, T. J. and Clark, J. P., 2007, "Predicting Transition in Turbomachinery, Part I – A Review and New Model Development," ASME *J. of Turbomachinery*, Vol. 129, pp. 1-13.

[13] Vanderplaats, G. N., 1984, Numerical Optimization Techniques for Engineering Design: With Applications, McGraw-Hill, New York.

[14] Santner, T. J., Williams, B. J., and Notz, W. I., 2003, The Design and Analysis of Computer Experiments, Springer-Verlag, New York.

[15] Walters, D.K., and Leylek, J.H., 2004, "A New Model for Boundary Layer Transition Using a Single-Point RANS Approach," *J. of Turbomachinery*, Vol. 126, pp. 193-202.

[16] Walters, K.K., and Leylek, J.J., 2005, "Computational Fluid Dynamics Study of Wake-Induced Transition on a Compressor-Like Flat Plate," *J. of Turbomachinery*, Vol. 127, pp. 52-63.

[17] Schlichting, H. and Gersten, K., 2000, “Boundary Layer Theory,” 8th Edition. New York, New York: Springer-Verlag.
[18] Sanders, D.D., O‟Brien, O.F., Sondergaard, R., Polanka, M.D., and Rabe, D.C., 2011, “Predicting Separation and Transitional Flow in Turbine Blades at Low Reynolds Numbers--Part I: Development of Prediction Methodology,” *J. of Turbomachinery*, Vol. 133, pp. 031011-1:031011-10.
[19] Sanders, D.D., O‟Brien, O.F., Sondergaard, R., Polanka, M.D., and Rabe, D.C., 2009, “A Mixing Plane Model Investigation of Separation and Transitional Flow at Low Reynolds Numbers in a Multistage Low Pressure Turbine,” AIAA Paper 2009-1467.
[20] Cutrone, L., De Palma, P., Pascazio, G., and Napolitano, M., 2007, “An Evaluation of Bypass Transition Models for Turbomachinery Flows,” *International Journal of Heat and Fluid Flow*,” Vol. 28, pp. 161-177.
[21] Baldwin, B., and Lomax, H., 1978, “Thin Layer Approximation and Algebraic Model for Separated Turbulent Flows,” AIAA Paper No. AIAA-78-257.
[22] Praisner, T.J., Grover, E.A., Rice, M.J., and Clark, J.P., 2007, “Predicting Transition in Turbomachinery-Part II: Model Validation and Benchmarking,” *J. of Turbomachinery*, Vol. 129, pp. 14-22.
[23] Bons, J.P., Sondergaard, R., and Rivir, R., 2001, “The Fluid Dynamics of LPT Blade Separation Control Using Pulsed Jets,” ASME Paper No GT-2001-0190.
[24] Binder, A., Schröder, T.H., and Hourmouziadis, J., 1988, “Turbulence Measurements in a Multistage Low-Pressure Turbine,” ASME Paper No. 88-GT-79.
[25] Schmitz, J.T., Morris, S.C., Ma, R., Corke, T.C., Clark, J.P., Kock, P.J., and Puterbaugh, S.L., 2010, “Highly Loaded Low-Pressure Turbine: Design, Numerical, and Experimental Analysis,” ASME Paper GT2010-23591.
[26] Lekakis, I.C., Adrian, R.J., and Jones, B.G., 1989, “Measurement of Velocity Vectors with Orthogonal and Non-Orthogonal Triple-Sensor Probes,” *Experiments in Fluids*, Vol. 7, pp. 228-240.
[27] Tritton, D.J, 1988, “Physical Fluid Dynamics,” 2nd Edition. New York, New York: Oxford University Press.
[28] Kline, S.J., and McClintock, F.A., 1953, “Describing Uncertainties in Single Sample Experiments,” *Mechanical Engineering*, Vol. 75.
[29] Roach, P.E., 1986, “The Generation of Nearly Isotropic Turbulence by Means of Grids,” *International Journal of Heat and Fluid Flow*, pp. 82-92.
[30] Shih, T.H., Liou, W.W., Shabbir, A., Yang, Z., and Zhu, J., 1995, “A New k-ε Eddy-Viscosity Model for High Reynolds Number Turbulent Flows-Model Development and Validation,” *Computers and Fluids*, Vol. 24 (No. 3), pp. 227-238.
[31] Weiss, A.P., and Fottner, L., 1995, “The Influence of Load Distribution on Secondary Flow in Straight Turbine Cascades,” *J. of Turbomachinery*, Vol. 117, pp. 133-141.
[32] Wilcox, D.C., 1998, “Turbulence Modeling for CFD,” 2nd Edition. La Cañada, California: DCW Industries Inc.
[33] Pope, S.B., 2000, “Turbulent Flows,” 1st Edition. Cambridge, UK: Cambridge University Press.
[34] Hunt, J.C.R., and Carruthers, D.J., 1990, “Rapid Distortion Theory and the „Problems‟ of Turbulence,” *J. of Fluid Mechanics*, Vol. 212, pp. 497-532.
[35] Goldstein, M.E., and Durbin, P.A., 1980, “The Effect of Finite Turbulence Spatial Scale on the Amplification of Turbulence by a Contracting Stream,” *J. of Fluid Mechanics*, Vol. 98, pp. 473-508.